IC/99/1
hep-ph/9901389
January 1999

Effects of the supersymmetric phases on the neutral Higgs sector

D. A. Demir [1]

The Abdus Salam International Center for Theoretical Physics, I-34100, Trieste, Italy

Abstract

By using the effective potential approximation and taking into account the dominant top quark and scalar top quark loops, radiative corrections to MSSM Higgs potential are computed in the presence of the supersymmetric CP–violating phases. It is found that, the lightest Higgs scalar remains essentially CP–even as in the CP–invariant theory whereas the other two scalars are heavy and do not have definite CP properties. The supersymmetric CP–violating phases are shown to modify significantly the decay rates of the scalars to fermion pairs.

[1]e-mail: ddemir@ictp.trieste.it

1 Introduction

The Minimal Supersymmetric Standard Model (MSSM) consists of various soft supersymmetry breaking parameters as well as the Higgsino mass parameter, μ, coming from the superpotential. In general, there is no a priori reason for taking all these parameters real, and thus, Yukawa couplings, gaugino masses, trilinear Higgs–sfermion couplings, A_f, Higgs bilinear coupling, $m_3^2 \equiv \mu B$, and μ– parameter itself can all be complex. On the other hand, the MSSM Lagrangian has two global symmetries $U(1)_{PQ}$ (Peccei-Quinn symmetry) and $U(1)_{R-PQ}$ (an R symmetry) under which all fields and parameters are charged. The selection rules for these symmetries limit the combinations of dimensionful parameters that can appear in a physical quantity so that one has, in fact, only three of these phases physical [1, 2]. Without loss of generality, these three physical phases can be identified with (1) the phase in the Cabibbo–Kobayashi–Maskawa matrix, δ_{CKM}, (2) $\varphi_\mu \equiv \mathcal{A}rg(\mu)$, and (3) $\varphi_{A_f} \equiv \mathcal{A}rg(A_f)$. Thus any physical quantity $\mathcal{F}$ has an explicit dependence on these phases: $\mathcal{F} = \mathcal{F}(\delta_{CKM}, \varphi_\mu, \varphi_{A_f})$.

Despite their presence in the Lagrangian, the phenomenological relevance of these CP–violating phases has often been questioned due to the smallness of the neutron and electron electric dipole moments [1, 3] which require them to be at most $\mathcal{O}(10^{-3})$. However, recent studies have shown that it is possible to suppress neutron and electron dipole moments without requiring these CP-violating phases to be small by allowing the existence of either non-universal soft breaking parameters at the unification scale [4] or some kind of cancellation among various supersymmetric contributions [5], or heavy enough sfermions for the first two generations [6]. In fact, following the last scenario, it was recently shown that the CP–violation in B– and K–systems can be saturated with φ_μ and φ_{A_f} only [7]. Apart from electric dipole moments and weak decays, these phases play a crucial role in the creation of the baryon asymmetry of the universe at the electroweak phase transition [8].

In this work, assuming that the electric dipole moments are suppressed by one of the methods metioned above, we take supersymmetric phases unconstrained, and investigate their effects on the Higgs sector of the MSSM. At the tree-level the Higgs sector of the MSSM conserves CP due to the fact that the superpotential is holomorphic in superfields entailing the absence

of flavour changing neutral currents and scalar–pseudoscalar mixings. When the supersymmetric phases φ_μ and φ_{A_f} vanish Higgs sector conserves CP at any loop order. In fact, the CP–conserving Higgs sector has been analyzed by several authors with the main purpose of evaluating the mass of the lightest Higgs boson which has the tree-level upper bound of M_Z. It has been found that radiative corrections, dominated by top and stop loops, elevate the tree-level bound significantly [9]. These one-loop results [9] have been improved by utilizing complete one-loop on-shell renormalization [10], renormalization group methods [11], diagrammatic methods with leading order QCD corrections [12], and two-loop on-shell renormalization [13]. However, when the supersymmetric phases are non-vanishing, as the recent studies have shown [14], the Higgs sector become CP– violating through the radiative corrections. As in the CP–conserving case, the radiative corrections will be dominated by the top and stop loops. Below we investigate effects of the supersymmetric phases on the Higgs masses, scalar-pseudoscalar mixings, and decay properties of scalars to fermion pairs. In doing this, we shall calculate one-loop radiative corrections coming from top and stop loops in the effective potential approximation.

This work is organized as follows. In Sec. 2 we compute the one-loop effective potential using top quark and stop contributions together with the specification of the particle spectrum and mixings. In Sec. 3 we discuss, as an example, the decay properties of the Higgs scalars to fermion pairs. In Sec. 4 we conclude the work.

2 Effective potential

The Higgs sector of the MSSM consists of two SU(2) doublets H_1, H_2 with opposite hypercharges $Y_1 = -1$, $Y_2 = +1$, and non-vanishing vacuum expectation values v_1, v_2. Allowing a finite alignment, θ, between the two Higgs doublets, we adopt the following decomposition:

$$\begin{aligned} H_1 &= \begin{pmatrix} H_1^0 \\ H_1^- \end{pmatrix} = \frac{1}{\sqrt{2}} \begin{pmatrix} v_1 + \phi_1 + i\varphi_1 \\ H_1^- \end{pmatrix} \\ H_2 &= \begin{pmatrix} H_2^+ \\ H_2^0 \end{pmatrix} = \frac{e^{i\theta}}{\sqrt{2}} \begin{pmatrix} H_2^+ \\ v_2 + \phi_2 + i\varphi_2 \end{pmatrix} . \end{aligned} \tag{1}$$

At the tree level the Higgs sector is described by the scalar potential

$$\begin{aligned} V_0(H_1,H_2) &= m_1^2|H_1|^2 + m_2^2|H_2|^2 + (m_3^2 H_1\cdot H_2 + H.c.) \\ &+ \frac{\lambda_1}{2}|H_1|^4 + \frac{\lambda_2}{2}|H_2|^4 + \lambda_{12}|H_1|^2|H_2|^2 + \tilde{\lambda}_{12}|H_1\cdot H_2|^2 \end{aligned} \quad (2)$$

with the parameters

$$\begin{aligned} m_1^2 &= m_{\tilde{H}_1}^2 + |\mu|^2\ ,\ m_2^2 = m_{\tilde{H}_2}^2 + |\mu|^2\ ,\ m_3^2 = |\mu B|\ ,\ \lambda_1 = \lambda_2 = (g_2^2+g_1^2)/4 \\ \lambda_{12} &= (g_2^2 - g_1^2)/4\ ,\ \tilde{\lambda}_{12} = -g_2^2/2 \end{aligned} \quad (3)$$

where $m_{\tilde{H}_{1,2}}^2$ and B are the soft supersymmetry breaking parameters. As is seen from (3), the tree level potential is described by real parameters; thus, the alignment between the two doublets can, in fact, be rotated away. Since, in the minimum, the potential is to have vanishing gradients in all directions, in particular, $\partial V_0/\partial\varphi_{1,2} = m_3^2\sin\theta = 0$, one automatically gets $\theta = 0$. Those terms of the tree level potential (2) quadratic in the components of the Higgs doublets (1) give the mass-squared matrix of neutral scalars the diagonalization of which yields the CP=-1 boson $A^0 = \cos\beta\varphi_1 - \sin\beta\varphi_2$ with mass $M_{A^0}^2 = -m_3^2/\sin\beta\cos\beta$, and two CP=+1 bosons which are linear combinations of ϕ_1 and ϕ_2 with a mixing angle α. The mixing angle α and the masses of the CP even scalars h and H are given by [15]

$$\tan 2\alpha = \frac{M_{A^0}^2 + M_Z^2}{M_{A^0}^2 - M_Z^2}\tan 2\beta \quad (4)$$

$$M_{h(H)}^2 = \frac{1}{2}(M_{A^0}^2 + M_Z^2 - (+)\sqrt{(M_{A^0}^2+M_Z^2)^2 - 4M_{A^0}^2 M_Z^2\cos^2 2\beta}) \quad (5)$$

where $\tan\beta \equiv v_2/v_1$, and $M_Z^2 = (g_2^2+g_1^2)(v_1^2+v_2^2)/4$ in our convention. It is readily seen that for $\tan\beta \gtrsim 2$ one has $\beta \sim \pi/2$, $M_h \sim M_Z$ and $M_H \sim M_A$. However, it is known that radiative corrections elevate M_h (bounded by M_Z at the tree level) significantly [9] without modifying the mass degeneracy between H and A when the theory conserves CP. When, however, the CP–violating MSSM phases are switched on, the degeneracy between H and A can be lifted considerably as discussed in [14].

We now start computing the radiative corrections to the tree potential (2) in the presence of the CP–violating MSSM phases φ_{μ,A_f}. Our main concern will be the investigation of the masses and mixings of the scalars as a function of the CP–violating angles. These mixings could be CP–conserving

(like $h - H$ mixing in the CP–respecting limit) as well as CP–violating as we will discuss below. To evaluate the radiative corrections we follow the effective potential approximation where the tree-level potential (2) is added to the one-loop contributions having the famous Coleman-Weinberg [9, 16] form

$$\Delta V = \frac{1}{64\pi^2} Str\mathcal{M}^4(H_1, H_2)(\log \frac{\mathcal{M}^2(H_1, H_2)}{Q^2} - \frac{3}{2}) \tag{6}$$

where $Str \equiv \sum_J (-1)^{2J+1}(2J+1)$ is the usual supertrace, and $\mathcal{M}(H_1, H_2)$ is the Higgs field dependent mass matrix of particles. ΔV depends on the renormalization scale Q which is presumably around the weak scale. In evaluating ΔV one includes the contributions of vector bosons, Higg bosons and fermions as well as their supersymmetric partners gauginos, Higgsinos and sfermions. Among all these particles top quarks and scalar top quarks give the dominant contributions [9]. However, for very large $\tan\beta$ values bottom-sbottom and τ-stau systems can become important. Besides these, since the dependence of ΔV on the CP-violating phases φ_{μ,A_f} originates from only the Higgsino (through μ dependence) and sfermion (through μ and A_f dependence) mass matrices, these two particle species attain a seperate importance. However, if one wishes to include the Higgsino contribution, all particle species must be included since then precision of the computation rises to the level of gauge couplings. In the following we neglect the contributions of gauge couplings and restrict ourselves to moderate values of $\tan\beta$ so that, to a good approximation, the dominant terms in ΔV are given by top– stop system. This approximation is convenient in that it picks up the phase-sensitive dominant contributions to ΔV.

In $(\tilde{t}_L, \tilde{t}_R)$ basis stop mass-squared matrix, neglecting the D-term contributions, takes the form

$$M_{\tilde{t}} = \begin{pmatrix} M_{\tilde{L}}^2 + h_t^2|H_2^0|^2 & h_t(A_t H_2^0 - \mu^* H_1^{0*}) \\ h_t(A_t^* H_2^{0*} - \mu H_1^0) & M_{\tilde{R}}^2 + h_t^2|H_2^0|^2 \end{pmatrix} \tag{7}$$

where μ and A_t are complex, $M_{\tilde{L},\tilde{R}}^2$ are the soft mass-squareds of left– and right–handed stops, and h_t is the top Yukawa coupling. Denoting the eigenvalues of $M_{\tilde{t}}$ by $m_{\tilde{t}_{1,2}}^2$ and using $m_t^2 = h_t^2|H_2^0|^2$ the one-loop effective potential takes the form

$$V = V_0 + \frac{6}{64\pi^2}\left(\sum_{a=\tilde{t}_1,\tilde{t}_2} m_a^4(\log\frac{m_a^2}{Q^2} - \frac{3}{2}) - 2m_t^4(\log\frac{m_t^2}{Q^2} - \frac{3}{2})\right) . \tag{8}$$

We require this effective potential to be minimized at (v_1, v_2, θ) at which it has to have vanishing gradients in all directions and the masses of the Higgs scalars must be real positive. Gradients of the potential with respect to the charged components of the Higgs doublets automatically vanish as there is no charge breaking effects in the vacuum. On the other hand, extremization of V with respect to neutral components of the Higgs doublets yield

$$v_1(2m_1^2 + \lambda_1 v_1^2 + (\lambda_{12} + \tilde{\lambda}_{12})v_2^2) + 2m_3^2 v_2 \cos\theta + 2\left(\frac{\partial \Delta V}{\partial \phi_1}\right)_0 = 0 \quad (9)$$

$$v_2(2m_2^2 + \lambda_2 v_2^2 + (\lambda_{12} + \tilde{\lambda}_{12})v_1^2) + 2m_3^2 v_1 \cos\theta + 2\left(\frac{\partial \Delta V}{\partial \phi_2}\right)_0 = 0 \quad (10)$$

$$m_3^2 v_2 \sin\theta - \left(\frac{\partial \Delta V}{\partial \varphi_1}\right)_0 = 0 \quad (11)$$

$$m_3^2 v_1 \sin\theta - \left(\frac{\partial \Delta V}{\partial \varphi_2}\right)_0 = 0 \quad (12)$$

where the subscript "0" implies the substitution $\phi_1 = \phi_2 = \varphi_1 = \varphi_2 = 0$ in the corresponding quantity. Equations (9) and (10) come by no surprise as they are the counterparts of the ones occurring in the CP-conserving case. However, with $(\partial \Delta V/\partial \varphi_{1,2})_0 \neq 0$, equations (11) and (12) now imply a non-trivial solution for $\sin\theta$ unlike the CP-conserving case where these gradients indentically vanish and one automatically obtains a vanishing θ. After some algebra one can show that

$$\left(\frac{\partial \Delta V}{\partial \varphi_1}\right)_0 = \tan\beta \left(\frac{\partial \Delta V}{\partial \varphi_2}\right)_0 . \quad (13)$$

Therefore, equations (11) and (12) imply one and the same solution for θ

$$m_3^2 \sin\theta = \frac{1}{2}\beta_{h_t}|\mu||A_t| \sin\gamma f(m_{\tilde{t}_1}^2, m_{\tilde{t}_2}^2) \quad (14)$$

where $\beta_{h_t} = (3h_t^2)/16\pi^2$, $\gamma = \varphi_\mu + \varphi_{A_t}$, and

$$f(x,y) = -2 + \log\frac{xy}{Q^4} + \frac{y+x}{y-x}\log\frac{y}{x} \quad (15)$$

is a scale-dependent one-loop function. Actually, if one uses the decomposition of the Higgs doublets in (1), in all one-loop formulae γ gets replaced by $\gamma + \theta$. However, since θ itself is a loop-induced quantity, its appearence together with γ is a two– and higher– loop effect which we neglect. Thus,

when computing ΔV we drop θ from (1) knowing that it is induced through (14). It is readily seen from (14) that unless γ vanishes θ remains finite. Furthermore, due to the form of the stop mass-squared matrix, all one-loop quantities turn out to depend on the combination $\gamma = \varphi_\mu + \varphi_{A_t}$. Of course, had we included the Higgsino contributions there would be terms that depend solely on φ_μ destructing this kind of relation. However, they would be subleading compared to top and stop contributions discussed here.

In (14) and all formulae below $m^2_{\tilde{t}_{1,2}}$ denote stop mass-squared eigenvalues evaluated at the minimum of the potential:

$$m^2_{\tilde{t}_{1,2}} = \frac{1}{2}\left(M^2_{\tilde{L}} + M^2_{\tilde{R}} + 2m^2_t \mp \Delta^2_{\tilde{t}}\right) \tag{16}$$

where

$$\Delta^2_{\tilde{t}} = \sqrt{(M^2_{\tilde{L}} - M^2_{\tilde{R}})^2 + 4m^2_t(|A_t|^2 + |\mu|^2\cot^2\beta - 2|\mu||A_t|\cot\beta\cos\gamma)}\ . \tag{17}$$

As usual, construction of the mass-squared matrix of the Higgs scalars proceeds through the evaluation of

$$M^2 = \left(\frac{\partial^2 V}{\partial\chi_i\partial\chi_j}\right)_0 \text{, where } \chi_i \in \mathcal{B} = \{\phi_1, \phi_2, \varphi_1, \varphi_2\}\ . \tag{18}$$

Solving $m^2_{1,2}$ from the stationarity conditions (9) and (10), and replacing them in M^2 one observes that, in the basis $\mathcal{B}$, the vector $\{0, 0, -\cos\beta, \sin\beta\}$ corresponds to the Goldstone mode G^0 eaten by Z boson to acquire its mass. Then in the reduced basis $\mathcal{B}' = \{\phi_1, \phi_2, \sin\beta\varphi_1 + \cos\beta\varphi_2\}$ the mass-squared matrix of the Higgs scalars becomes

$$M^2 = \begin{pmatrix} M^2_Z c^2_\beta + \tilde{M}^2_A s^2_\beta + \Delta_{11} & -(M^2_Z + \tilde{M}^2_A)s_\beta c_\beta + \Delta_{12} & r\Delta \\ -(M^2_Z + \tilde{M}^2_A)s_\beta c_\beta + \Delta_{12} & M^2_Z s^2_\beta + \tilde{M}^2_A c^2_\beta + \Delta_{22} & s\Delta \\ r\Delta & s\Delta & \tilde{M}^2_A + \Delta \end{pmatrix} \tag{19}$$

where $c_\beta = \cos\beta$ and $s_\beta = \sin\beta$. The scalar mass-squared matrix involves various parameters whose explicit expressions we list below. The adimensional parameters r and s are given by

$$r = -\frac{\sin\beta}{\sin\gamma}\frac{|A_t|\cos\gamma - |\mu|\cot\beta}{|A_t|} \tag{20}$$

$$\begin{aligned} s &= \frac{\sin\beta}{\sin\gamma}\frac{1}{|\mu||A_t|g(m^2_{\tilde{t}_1}, m^2_{\tilde{t}_2})}(|A_t|(|A_t| - |\mu|\cot\beta\cos\gamma)g(m^2_{\tilde{t}_1}, m^2_{\tilde{t}_2}) \\ &- (m^2_{\tilde{t}_2} - m^2_{\tilde{t}_1})\log\frac{m^2_{\tilde{t}_2}}{m^2_{\tilde{t}_1}})\ . \end{aligned} \tag{21}$$

While r originates mainly from the stop left-right mixings, s has an additional term depending on the the stop mass splitting $\log \frac{m^2_{\tilde{t}_2}}{m^2_{\tilde{t}_1}}$.

The parameters of mass dimension can be expressed as follows

$$\Delta = -2\beta_{h_t} \frac{\sin^2\gamma}{\sin^2\beta} \frac{|\mu|^2 |A_t|^2 m_t^2}{(m^2_{\tilde{t}_2} - m^2_{\tilde{t}_1})^2} g(m^2_{\tilde{t}_1}, m^2_{\tilde{t}_2}) \tag{22}$$

$$\Delta_{11} = -2\beta_{h_t} \frac{|\mu|^2 m_t^2 (|A_t|\cos\gamma - |\mu|\cot\beta)^2}{(m^2_{\tilde{t}_2} - m^2_{\tilde{t}_1})^2} g(m^2_{\tilde{t}_1}, m^2_{\tilde{t}_2}) \tag{23}$$

$$\begin{aligned} \Delta_{12} &= -2\beta_{h_t} |\mu| m_t^2 \{ \frac{|A_t|\cos\gamma - |\mu|\cot\beta}{(m^2_{\tilde{t}_2} - m^2_{\tilde{t}_1})} \log \frac{m^2_{\tilde{t}_2}}{m^2_{\tilde{t}_1}} \\ &- \frac{|A_t|[(|A_t|\cos\gamma - |\mu|\cot\beta)^2 + |A_t|(|A_t| - |\mu|\cot\beta)\sin^2\gamma]}{(m^2_{\tilde{t}_2} - m^2_{\tilde{t}_1})^2} \\ &\times g(m^2_{\tilde{t}_1}, m^2_{\tilde{t}_2}) \} \end{aligned} \tag{24}$$

$$\begin{aligned} \Delta_{22} &= 2\beta_{h_t} m_t^2 \{ \log \frac{m^2_{\tilde{t}_2} m^2_{\tilde{t}_1}}{m_t^4} + \frac{2|A_t|(|A_t| - |\mu|\cot\beta\cos\gamma)}{(m^2_{\tilde{t}_2} - m^2_{\tilde{t}_1})} \log \frac{m^2_{\tilde{t}_2}}{m^2_{\tilde{t}_1}} \\ &- \frac{|A_t|^2 (|A_t| - |\mu|\cot\beta\cos\gamma)^2}{(m^2_{\tilde{t}_2} - m^2_{\tilde{t}_1})^2} g(m^2_{\tilde{t}_1}, m^2_{\tilde{t}_2}) \} \end{aligned} \tag{25}$$

where the function $g(m^2_{\tilde{t}_1}, m^2_{\tilde{t}_2})$ in these expressions reads

$$g(x,y) = f(x,y) - \log \frac{xy}{Q^4}. \tag{26}$$

Therefore, unlike $f(m^2_{\tilde{t}_1}, m^2_{\tilde{t}_2})$, $g(m^2_{\tilde{t}_1}, m^2_{\tilde{t}_2})$ does not have an explicit dependence on the renormalization scale Q. In fact, the adimensional parameters r and s as well as the mass parameters (21)-(24) have no explicit dependence on Q. On the other hand, the remaining mass parameter, $\tilde{M}_A^2$, in the scalar mass-squared matrix (19) is an explicit function of Q:

$$\tilde{M}_A^2 = \frac{m_3^2}{\sin\beta\cos\beta} \frac{\sin(\theta - \gamma)}{\sin\gamma} \ . \tag{27}$$

It is the θ (13) dependence of $\tilde{M}_A^2$ that makes it Q-dependent. However, the explicit Q dependence of θ should cancel with the implicit Q dependence of $\tan\beta$ and m_3^2 to make $\tilde{M}_A^2$ scale-independent [9].

According to the decomposition of Higgs doublets in (1), ϕ_1 and ϕ_2 are of CP=+1 whereas $\sin\beta\varphi_1 + \cos\beta\varphi_2$ is of CP=-1. As suggested by the form of the scalar mass-squared matrix (19) there are mainly two kinds of mixings: (1) mixing of the scalars with different CP induced by $M^2_{13} = r\Delta$

and $M^2_{23} = s\Delta$, and (2) mixing of the CP=+1 scalars through $M^2_{12} = -(M^2_Z + \tilde{M}^2_A)s_\beta c_\beta + \Delta_{12}$. While the former are induced purely by the non-vanishing supersymmetric phases the latter exists in the CP–respecting limit too. In the CP–conserving limit, that is, $\sin\gamma \to 0$, one obtains $r\Delta \to 0$, $s\Delta \to 0$ and $\Delta \to 0$. In this case CP=+1 and CP=-1 sectors in (19) decouple and reproduce the particle spectrum of the CP– conserving limit in which $\tilde{M}_A$ becomes the radiatively corrected pseudoscalar mass, and $\Delta_{11,12,22}$ become the usual one-loop contributions [9] to the CP=+1 scalar mass-squared matrix. For a proper interpretation of results of the numerical analysis below it is convenient to know the relative strengths of the CP–violating and conserving mixings. For large $\tan\beta$ equations (20) and (21) go over to

$$r \sim -\cot\gamma\ , \quad s \sim \frac{1}{\sin\gamma}\left(\frac{|A_t|}{|\mu|} + \frac{4(m^2_t + M^2_Q)}{|\mu||A_t|}\right) \tag{28}$$

where we assumed $M_{\tilde{L}} \sim M_{\tilde{R}} \equiv M^2_Q >> m_t|A_t|$ and $|A_t| >> |\mu|\cot\beta$ in derivation. Equation (28), thus, implies that $|r|/|s| << 1$. This follows mainly from the dependence of the stop mass-matrix (7) on H^0_2 which causes not only $|s\Delta|$ but also $|\Delta_{12}|$ and $|\Delta_{22}|$ to be larger than $|\Delta_{11}|$ and $|r\Delta|$ through stop and stop-top splittings. An immediate consequence of (28) is that one eigenstate of the scalar mass-squared matrix (19) will be of mainly CP=+1. Thus one expects that among the three mass eigenstate scalars one will continue to have CP=+1 with a small CP=-1 component while the other two can mix significantly depending on the relative stregths of the other one-loop corrections. This observation can be justified numerically by analyzing the relative strengths of CP–violating and CP–conserving mixings as classified above. Fig.1 shows the variation of $M^2_{13}/|M^2_{12}|$ (solid curve) and $M^2_{23}/|M^2_{12}|$ (dashed curve) with $\tan\beta$ for $M_{\tilde{L}} = M_{\tilde{R}} = |A_t| = 10 \cdot M_Z$, $|\mu| = 2.5 \cdot M_Z$ and $\tilde{M}_A = 2 \cdot M_Z$ with $\gamma = \pi/4$. As the figure suggests larger the $\tan\beta$ bigger the CP–violating mixings compared to the mixing between the CP=+1 components. The increase of these ratios with $\tan\beta$ can be understood as follows: (1) $\beta \to \pi/2$ as $\tan\beta$ grows to higher values, and thus, $|-(M^2_Z + \tilde{M}^2_A)s_\beta c_\beta|$ decreases gradually, (2) Δ_{12} is positive for these parameters (and even for higher values of $|\mu|$ due to $\cot\beta$ suppression) and grows with $\tan\beta$ due to $\log m^2_{\tilde{t}_2}/m^2_{\tilde{t}_1}$ so that M^2_{12} decreases with increasing $\tan\beta$, and the ratios increase gradually since M^2_{13} and M^2_{23} decrease with $\tan\beta$ more slowly.

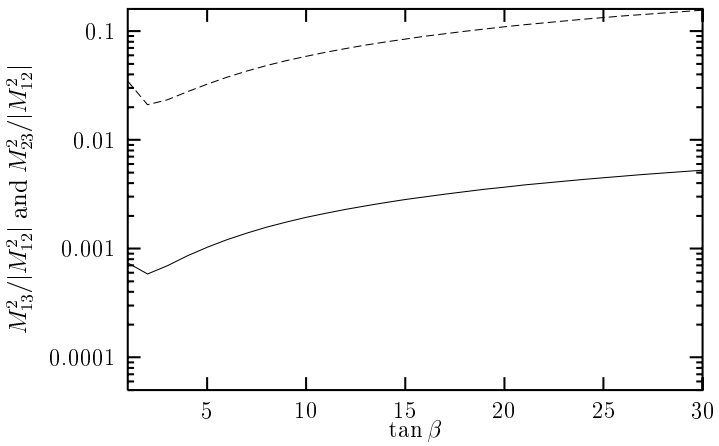

Figure 1: Variation of $M^2_{13}/|M^2_{12}|$ (solid curve) and $M^2_{23}/|M^2_{12}|$ (dashed curve) with $\tan\beta$ for $M_{\tilde{L}} = M_{\tilde{R}} = |A_t| = 10{\cdot}M_Z$, $|\mu| = 2.5{\cdot}M_Z$ and $\tilde{M}_A = 2{\cdot}M_Z$ with $\gamma = \pi/4$. The CP– violating mixings become important for large $\tan\beta$.

In Fig. 1 we plot ratios of the CP–violating mixings to CP–conserving ones; however, if one plots CP–violating mixings directly, for example in units of $(10 \cdot M_Z)^2$ for $|\mu| = 10 \cdot M_Z$, $\gamma = \pi/2$ and $\tilde{M}_A = 5 \cdot M_Z$, in absolute magnitude, M^2_{13} (M^2_{23}) starts with $\sim 4 \cdot 10^{-2}$ ($\sim 10^{-2}$) at $\tan\beta = 2$ and falls down $3 \cdot 10^{-5}$ ($2 \cdot 10^{-4}$) at $\tan\beta \sim 30$. These results generally agree with those of [14] though the computational schemes are different.

Since the parameter space is too wide to cover fully, in the following we restrict ourselves to the following set

$$M_{\tilde{L}} = M_{\tilde{R}} = 500\,\mathrm{GeV}\ , |A_t| = 1\,\mathrm{TeV}\ , |\mu| = 250\,\mathrm{GeV}\ , \tilde{M}_A = 200\,\mathrm{GeV} \quad (29)$$

and vary γ over its full range. Each time we consider low and high $\tan\beta$ regimes seperately by taking $\tan\beta = 4$ and 30. As $\tan\beta$ increases $|\mu|\cot\beta$ decreases, and this enhances the contribution of the radiative corrections. However, variation with $\tan\beta$ is not the whole story because even for $\cot\beta \rightsquigarrow 0$, Δ, Δ_{11}, Δ_{12} are proportional to $|\mu||A_t|$ so that choice for the latter affects

the strength of the radiative corrections. Especially for large $\tan\beta$, stop masses weakly depend on $|\mu|$; therefore, these elements of the mass-squared matrix become more sensitive to the choice for $|\mu|$. The parameter set (29) is a moderate choice in that it enhances the radiative corrections through large $|A_t|$ term without causing too big splittings among the the Δ coefficients in (22)-(25) thanks to the relatively small $|\mu|$ term. Dependence on the parameter $\tilde{M}_A$ is as in the CP–invariant theory, namely, heavy scalars have masses around $\tilde{M}_A$.

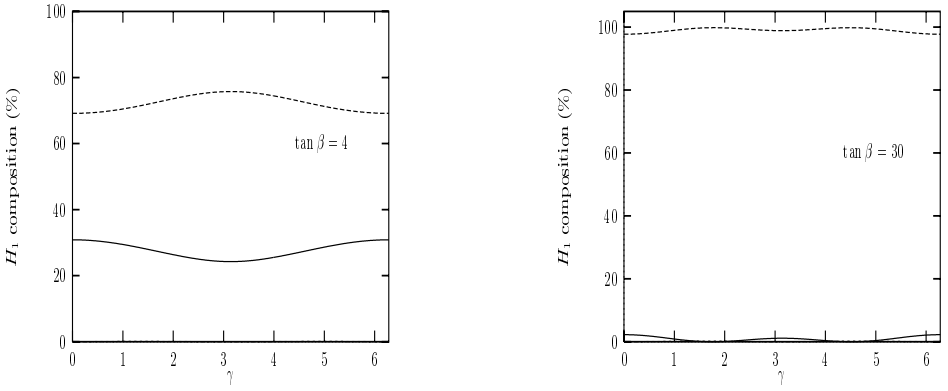

Figure 2: Percentage composition of H_1 as a function of γ for $\tan\beta = 4$ (left panel) and $\tan\beta = 30$ (right panel). Here ϕ_1, ϕ_2 and $\sin\beta\varphi_1 + \cos\beta\varphi_2$ contributions are $|\mathcal{R}_{11}|^2$ (solid curve), $|\mathcal{R}_{12}|^2$ (dashed curve) and $|\mathcal{R}_{13}|^2$ (short-dashed curve), in percents. Values of the parameters are given in (29).

In principle one can diagonalize analytically the scalar mass-squared matrix (19); however, the results will be too complicated to be suggestive. Instead of using such oblique expressions we shall fix the notation for diagonalization and numerically analyze the results. The scalar mass-squared matrix (19) can be diagonalized by a similarity transformation

$$\mathcal{R}\cdot M^2\cdot\mathcal{R}^T = diag.(M^2_{H_1}, M^2_{H_2}, M^2_{H_3})\ , \text{where } \mathcal{R}\cdot\mathcal{R}^T = 1 \qquad (30)$$

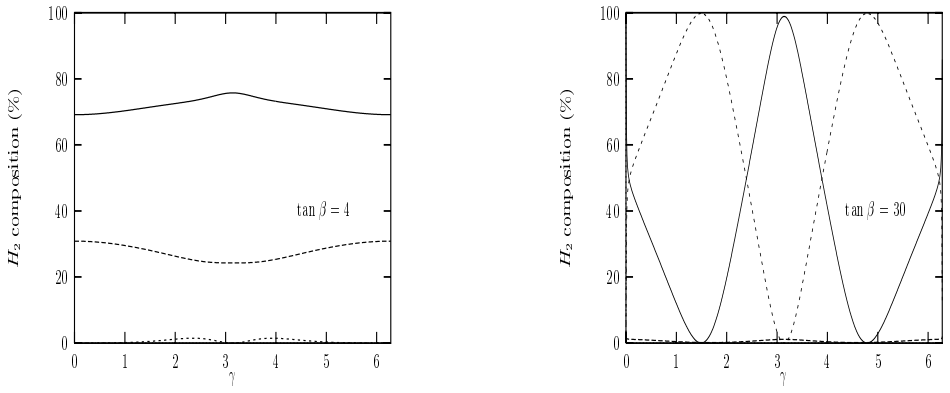

Figure 3: Percentage composition of H_2 as a function of γ for $\tan\beta = 4$ (left panel) and $\tan\beta = 30$ (right panel). Here ϕ_1, ϕ_2 and $\sin\beta\varphi_1 + \cos\beta\varphi_2$ contributions are $|\mathcal{R}_{21}|^2$ (solid curve), $|\mathcal{R}_{22}|^2$ (dashed curve) and $|\mathcal{R}_{23}|^2$ (short-dashed curve), in percents.

where the mass- eigenstate scalar fields are defined by

$$\begin{pmatrix} H_1 \\ H_2 \\ H_3 \end{pmatrix} = \mathcal{R} \cdot \begin{pmatrix} \phi_1 \\ \phi_2 \\ \sin\beta\varphi_1 + \cos\beta\varphi_2 \end{pmatrix} . \tag{31}$$

γ– dependence of the elements of $\mathcal{R}$ is crucial for determining the CP– impurity of the mass eigenstate scalars H_i. In analyzing $\mathcal{R}$ we adopt a convention such that in the limit of vanishing $\sin\gamma$ we let $H_1 \to h$, $H_2 \to H$ and $H_3 \to A$, that is, H_1 is the lightest Higgs. We expect results of the CP–invariant theory be recovered at the CP–conserving points $\gamma = 0, \pi, 2\pi$ except for γ–dependence of various parameters.

Depicted in Fig. 2 is the γ– dependence of H_1 composition in percents for the parameter set in eq. (29). From the left panel we observe that, on the average, H_1 has $\sim 30\%$ ϕ_1 and $\sim 70\%$ ϕ_2 composition. As is immediate from the figure, CP=-1 component of H_1 is small, in fact, it never exceeds 0.02%

in the entire range of γ. From the right panel, however, we observe that ϕ_2 contribution rises near to 100% line, and correspondingly, ϕ_1 contribution remains below 2.5%. This result is a consequence of $\beta \to \pi/2$ limit reminescent from the CP–invariant theory. In this large $\tan\beta$ limit, $\sin\beta\varphi_1 + \cos\beta\varphi_2$ composition of H_1 reaches at most to 0.2% over the entire range of γ. It is clear that both windows of the figure suggest that the lightest Higgs remains essentially a CP–even Higgs scalar for the parameter space in (29).

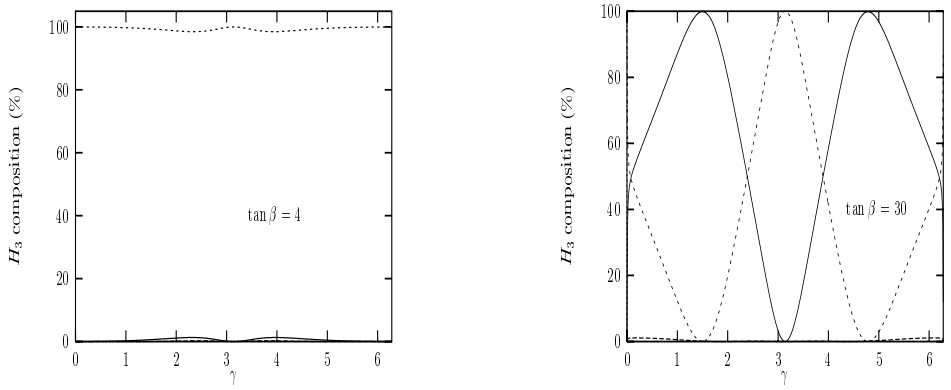

Figure 4: Percentage composition of H_3 as a function of γ for $\tan\beta = 4$ (left panel) and $\tan\beta = 30$ (right panel). Here ϕ_1, ϕ_2 and $\sin\beta\varphi_1 + \cos\beta\varphi_2$ contributions are $|\mathcal{R}_{31}|^2$ (solid curve), $|\mathcal{R}_{32}|^2$ (dashed curve) and $|\mathcal{R}_{33}|^2$ (short-dashed curve), in percents.

In Fig. 3 we show the percentage composition of H_2 as a function of γ for $\tan\beta = 4$ (left panel) and $\tan\beta = 30$ (right panel). In agreement with the left panel of Fig. 2, for $\tan\beta = 4$ (left panel) H_2 has $\sim 70\%$ ϕ_1 and $\sim 30\%$ ϕ_2 composition. Unlike H_1, however, $\sin\beta\varphi_1 + \cos\beta\varphi_2$ composition of H_2 becomes as large as 1.3%. As expected, this increase in the CP=-1 component is compansated by H_3. More spectacular side of Fig. 3 arises for large $\tan\beta$ (right panel) in which H_2 is seen to gain non-negligible CP–odd

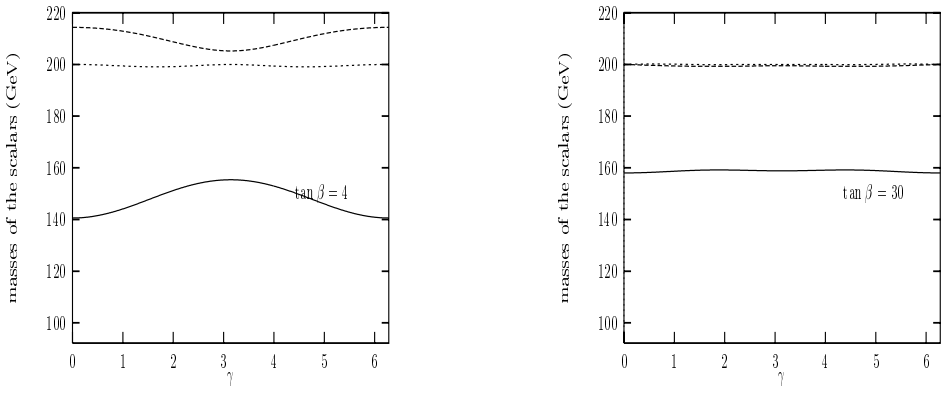

Figure 5: Masses of the scalars H_i as a function of γ for $\tan\beta = 4$ (left panel) and $\tan\beta = 30$ (right panel). Here M_{H_1}, M_{H_2} and M_{H_3} are shown by solid, dashed, and short-dashed curves, respectively. In both panels H_1 is the lightest scalar whose composition is shown in Fig. 2.

composition. In accordance with large $\tan\beta$ limit described by eq. (28) there is a strong dependence γ. Sum of ϕ_1 and ϕ_2 compositions of H_2 starts from $\gamma = 0$ at 100% line, and the former is diminished rather fast until $\gamma = \pi/2$. Beyond this point it rises rapidly to 98% line at $\gamma = \pi$ where its CP=+1 component completes to 100% in accordance with the CP conservation. One notes the complementary behaviour of $\sin\beta\varphi_1 + \cos\beta\varphi_2$ composition which, in particular, implies that H_2 is a pure pseudoscalar around $\gamma = \pi/2$.

Depicted in Fig. 4 is the percentage composition of H_3 as a function of γ for $\tan\beta = 4$ (left panel) and $\tan\beta = 30$ (right panel). In agreement with the left panels of Figs. 2 and 3, H_3 is almost a pure pseudoscalar for $\tan\beta = 4$. On the other hand, for $\tan\beta = 30$ (right panel) H_3 is seen to loose its CP–purity in accordance with the right panel of Fig. 3. Thus H_3, except for the points discussed above, does not have definite CP characteristics. From Fig. 3 and Fig. 4 one concludes that heavy scalars have non-negligible

CP–impurity in agreemnet with the results of [14].

ϕ_1 (solid curve), ϕ_2 (dashed curve) and $\sin\beta\varphi_1 + \cos\beta\varphi_2$ (short-dashed curve) compositions of the Higgs fields H_i shown in Figs. 2-4 need further elaboration. In accordance with Fig. 1 CP–violating mixings are small for small $\tan\beta$ and one necessarily recovers the results of the CP–invariant theory where ϕ_1 and ϕ_2 mix with each other to form h^0 and H^0, and $\sin\beta\varphi_1 + \cos\beta\varphi_2$ is nothing but the psedoscalar A^0. Thus, in this limit mixings are as in the CP–invariant theory as is evident from the left panels of each figure. For large $\tan\beta$, however, each Higgs field undergoes certain variations in its compositions. First of all, dominant ϕ_2 composition of the light Higgs is easily understandable since the analog of the tree-level Higgs mixing angle (4) approaches $\beta + \pi/2 \approx \pi$ for large $\tan\beta$ [17]. The remaining component of H_1 comes mainly form ϕ_1 since CP–breaking contributions are small for this eigenvalue (See (28)). On the other hand, compositions of H_2 and H_3 are determined from large $\tan\beta$ (dominant ϕ_1 contribution to their CP–even parts) as well as the radiative corrections. As is evident from (28), in large $\tan\beta$ regime $M_{13} \sim \sin\gamma\cos\gamma$ and $M_{23} \sim \sin\gamma$ so that (for example) the zeroes of the components of H_2 follow certain combinations of these functional behaviours. The sharp changes in the ϕ_2 and $\sin\beta\varphi_1 + \cos\beta\varphi_2$ compositions of H_2 and H_3 at $\gamma = 0$ (for large $\tan\beta$) follows from the γ dependencies of M_{13} and M_{23} (See eq. (28)). Indeed, variation of the compositions near $\gamma = 0$ behaves roughly as $\sin 2\gamma \pm \sin\gamma$ which varies quite fast near the origin.

Until now in Figs. 2-4 we have discussed the CP properties of the eigenstates of the scalar mass-squared matrix (19). Now we analyze the γ dependence of the masses of these scalars for identifying their hierarchy. Fig. 5 shows the γ–dependence of the scalar masses for $\tan\beta = 4$ (left panel) and $\tan\beta = 30$ (right panel). It is clear that H_1 is the lightest scalar in both cases. Moreover, the small gap (at most $\sim 20\ GeV$) between M_{H_3} and M_{H_2} in the left panel is closed in the right panel where H_2 and H_3 are degenerate in mass. This behaviour occurs also in the CP–conserving case [15, 9] due to the large value of $\tan\beta$. One more thing about Fig. 5 is that the masses of H_2 and H_3 are almost completely determined by $\tilde{M}_A = 2 \cdot M_Z$. For instance, for $\tilde{M}_A = 10 \cdot M_Z$, H_2 and H_3 weigh approximately $10 \cdot M_Z$. Unlike this strong $\tilde{M}_A$– dependence of M_{H_3} and M_{H_2}, mixing among the Higgs scalars and lightest Higgs mass depends mainly on $\tan\beta$. The γ–dependence of the

masses around $\gamma = \pi$ (especially in the case of $\tan\beta = 4$) differ from those at other CP–conserving points due mainly to the minimization of the light stop mass (See eqs. (16) and (17)). Finally, one observes that the light Higgs mass is higher than the usual constrained MSSM bounds [18] due to the large value of A_t and relatively small soft stop masses which is not possible to produce through RGE's (except, possibly, with non-universal initial conditions).

From Figs. 2-5 one concludes that the lightest Higgs scalar remains essentially a CP=+1 scalar, and the remaining heavy scalars do not possess definite CP characteristics. In this sense, MSSM is seen to accomodate a light CP=+1 Higgs boson as in the CP–invariant case. In addition, the heavy indefinite CP Higgs scalars of the MSSM not only have no correspondent in the SM but also are distinguishable from the lightest Higgs due to both their masses and CP properties. In the next section we shall discuss decay properties of these Higgs scalars to fermions and investigate the deviations from the CP–conserving limit.

3 An example: Decays of the Higgs scalars to fermion pairs

The form of the scalar mass-squared matrix (19) as well as the mixing matrix $\mathcal{R}$ shows clearly the CP–violation in the Higgs sector. In general, all parameters of the Higgs sector turn out to depend on these CP–violating angles, for instance, $\tan\beta$, masses of scalars, stop masses are explicit functions of γ. In this sense couplings of the Higgs scalars to the MSSM particle spectrum are necessarily modified. Therefore, the CP–violating angle γ can show up, for example, in the rates for various collision processes testable at future colliders. As an example, one can consider an e^+e^- collider with sufficiently large center-of-mass energy. In such a collider one of the main Higgs production mechanisms is the Bjorken process $Z^* \to ZH_i$. When the center-of-mass energy is varied over a range of values including the masses of the scalars it is expected that the cross section, as a function of the invariant mass flow into H_i branch, should show three distinct peaks situated at the scalar masses M_{H_i}. Needless to say, in the CP– conserving case there would be two peaks instead of three.

We now discuss couplings of the scalars to fermion pairs in detail. That

the scalars H_i are devoid of definite CP properties influence their couplings to fermions significantly. Rephasing the fermion fields appropriately one can always make fermion masses real after which coupling of the scalar H_i to u-type quarks, d-type quarks and charged leptons take the form

$$H_i\bar{u}u \;:\; (\sqrt{2}G_F)^{1/2}\frac{m_u}{\sin\beta}(\mathcal{R}_{i2} + i\cos\beta\mathcal{R}_{i3}\gamma_5) \tag{32}$$

$$H_i\bar{d}d \;:\; (\sqrt{2}G_F)^{1/2}\frac{m_d}{\cos\beta}(\mathcal{R}_{i1} + i\sin\beta\mathcal{R}_{i3}\gamma_5) \tag{33}$$

$$H_i\bar{\ell}\ell \;:\; (\sqrt{2}G_F)^{1/2}\frac{m_\ell}{\cos\beta}(\mathcal{R}_{i1} + i\sin\beta\mathcal{R}_{i3}\gamma_5) \tag{34}$$

where one observes that each coupling picks up a γ_5 piece showing its CP=-1 content. Moreover, as the Feynman rules above dictate γ_5 piece is enhanced for large $\tan\beta$ ($\cot\beta$) for u-type quarks (d-type quarks and charged leptons). To have a quantitative understanding of the effects of γ on the Higgs decays to fermion pairs it is convenient to compute the ratio

$$\begin{aligned} R_{if} &= \frac{\Gamma(H_i \to \bar{f}f|\gamma \neq 0)}{\Gamma(H_i \to \bar{f}f|\gamma = 0)} \\ &= \frac{(\mathcal{R}_{iq})^2(1-4m_f^2/M_{H_i}^2)^{3/2} + a_f^2(\mathcal{R}_{i3})^2(1-4m_f^2/M_{H_i}^2)^{1/2}}{(\mathcal{R}_{iq}(0))^2(1-4m_f^2/M_{H_i}^2(0))^{3/2} + a_f^2(\mathcal{R}_{i3}(0))^2(1-4m_f^2/M_{H_i}^2(0))^{1/2}} \end{aligned} \tag{35}$$

where $q = 2(1)$ and $a_f = \cos\beta(\sin\beta)$ for u-type quarks (d-type quarks and charged leptons). The argument "0" of the quantities in the denominator implies the replacement $\gamma = 0$. It is clear that $\Gamma(H_i \to \bar{f}f)$ consists of phase space factors pertinent to both CP=+1 and CP=-1 cases seperately. According to the conventions we apply, for $i = 1, 2$ ($i = 3$) only the first (second) term survives in the denominator. The CP–violating MSSM phase, γ not only functions in creating the additional terms in the Feynman rules (31-33) but also affects the couplings and masses themselves.

We now perform a numerical computation of R_{if} for the parameter space used up to now. In particular, we concentrate on two cases $f = b$ and $f = c$, that is, we consider b- and c- quarks in the computation. Such an analysis will be exhaustive as it covers the cases listed (32)-(34). We start by listing the quantities $(\mathcal{R}_{ij}(0))^2$ necessary for computing R_{if} in Tables 1 and 2. Below, when speaking about the elements of the mixing matrices for $\gamma = 0$ we shall always refer to these tables.

Fig. 6 shows the γ–dependencies of R_{1b} and R_{1c} for $\tan\beta = 4$ (solid curve) and $\tan\beta = 30$ (dashed curve). Let us first discuss R_{1b} (left panel).

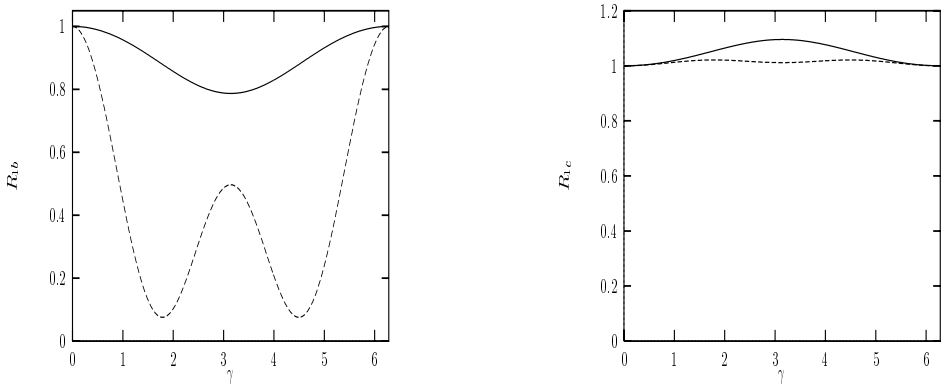

Figure 6: R_{1b} (left panel) and R_{1c} (right panel) defined in (34) as a function of γ for $\tan\beta = 4$ (solid curve) and $\tan\beta = 30$ (dashed curve).

As Fig. 2 shows ϕ_1 composition of H_1 starts with 0.31 at $\gamma = 0$ (See Table 1) and falls to 0.24 at $\gamma = \pi$. Therefore, R_{1b} falls to $0.24/0.31 = 0.77$ around $\gamma = \pi$. On the other hand, for $\tan\beta = 30$ R_{1b} obtains a relatively fast variation of R_{1b} with γ. This behaviour of R_{1b} follows from its ϕ_1 component in the right panel of Fig. 2, which takes the value of 1.1% around $\gamma = \pi$. Therefore, R_{1b} rises to $0.01/0.02 = 0.5$ at $\gamma = \pi$ as follows from Table 2. On the other hand, from the right panel of the figure one observes that, R_{1c} remains around its conterpart in the CP–conserving limit. Using Tables 1-2, and ϕ_2 compositions in Fig. 2 one can easily infer the behaviour of R_{1c}. In particular, constancy of $\tan\beta = 30$ curve follows from the constancy of the ϕ_2 composition in Fig. 2 (right panel).

Depicted in Fig. 7 is the dependence of R_{2b} (left panel) and R_{2c} (right panel) on γ for $\tan\beta = 4$ (solid curve) and $\tan\beta = 30$ (dashed curve). First concentrating on R_{2b}, one observes a slow variation with γ compared to the lightest Higgs (Fig. 6 (left panel)). The behaviour of $\tan\beta = 4$ curve simply follows from the ϕ_1 composition of H_2 in Fig. 3 (left panel). However, the flat

$(\mathcal{R}_{ij}(0))^2$	i=1	i=2	i=3
$(\mathcal{R}_{i1}(0))^2$	0.31	0.69	0.0
$(\mathcal{R}_{i2}(0))^2$	0.69	0.31	0.0
$(\mathcal{R}_{i3}(0))^2$	0.0	0.0	1.0

Table 1: Elements of the scalar mixing matrix entering the Feynman rules (32)-(34) for $\tan\beta = 4$ and γ=0. Here i (j) runs over H_i $(\phi_1, \phi_2, \sin\beta\varphi_1 + \cos\beta\varphi_2)$.

$(\mathcal{R}_{ij}(0))^2$	i=1	i=2	i=3
$(\mathcal{R}_{i1}(0))^2$	0.02	0.98	0.0
$(\mathcal{R}_{i2}(0))^2$	0.98	0.02	0.0
$(\mathcal{R}_{i3}(0))^2$	0.0	0.0	1.0

Table 2: Elements of the scalar mixing matrix entering the Feynman rules (32)-(34) for $\tan\beta = 30$ and $\gamma = 0$, with the same convention in Table 1.

behaviour of R_{2b} for large $\tan\beta$ follows from the complementary behaviour of its ϕ_1 and $\sin\beta\varphi_1 + \cos\beta\varphi_2$ compositions shown in Fig. 3 (right panel). It is with the $a_b = \sin\beta$ factor in eq. (35) that such a compensation between its opposite CP–components occur. The variation of R_{2c} follows from the ϕ_2 composition of H_2 Fig. 3 following the same lines of reasoning used in discussing R_{1b} above.

Finally, Fig. 8 shows the variation of R_{3b} (left panel) and R_{3c} (right panel) with γ for $\tan\beta = 4$ (solid curve) and $\tan\beta = 30$ (dashed curve). For $\tan\beta = 4$, both R_{3b} and R_{3c} remain around unity because of the fact that there is little $H - A$ mixing and $(\mathcal{R}_{33})^2(0) = 1$. That R_{3b} remains flat for $\tan\beta = 30$ follows from the interplay between its CP=+1 and CP=-1 components as in R_{2b}. On the other hand, R_{3c}, for $\tan\beta = 4$ follows simply from its vanishing ϕ_2 and 100% $\sin\beta\varphi_1 + \cos\beta\varphi_2$ components in Fig. 4 (left panel). Since ϕ_2 composition is negligibly small for large $\tan\beta$ (right panel of Fig. 4), variation of R_{3c} is mainly dictated by its CP=-1 component (short-dotted curve in the right panel of Fig. 4). For example, $R_{2c} = 1$ at $\gamma = \pi$ just due to its 100% composition in Fig. 4.

From the study of the decay rates of the Higgs particles to $\bar{b}b$ and $\bar{c}c$ pairs one concludes that their CP–impurity causes significant changes compared to the CP–invariant limit. In particular, one notes the enhancement in R_{3c}

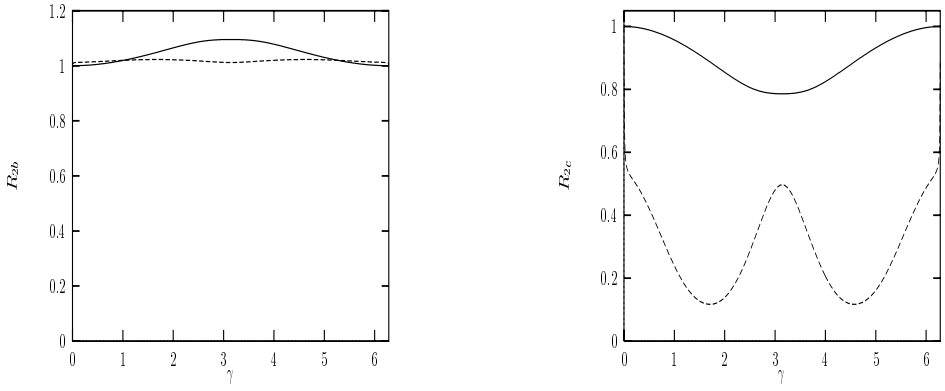

Figure 7: R_{2b} (left panel) and R_{2c} (right panel) defined in (34) as a function of γ for $\tan\beta = 4$ (solid curve) and $\tan\beta = 30$ (dashed curve).

near $\gamma = 0$ point, which is one order of magnitude above its value in the CP–conserving limit.

4 Conclusion and Discussions

In this work we have studied the possible effects of the supersymmetric CP–violating phases on the neutral Higgs scalars of the MSSM. We have adopted effective potential approximation in computing the radiative corrections and have taken into account only the dominant top quark and top squark loops. We now itemize the main results of the work:

- Radiative corrections induce an unremovable relative phase between the two Higgs doublets. This relative phase remains non-vanishing as long as the supersymmetric CP–violating phases are finite, and determines the dynamics of the electroweak phase transition [19].

- The CP=+1 and CP=-1 components of the Higgs doublets are mixed

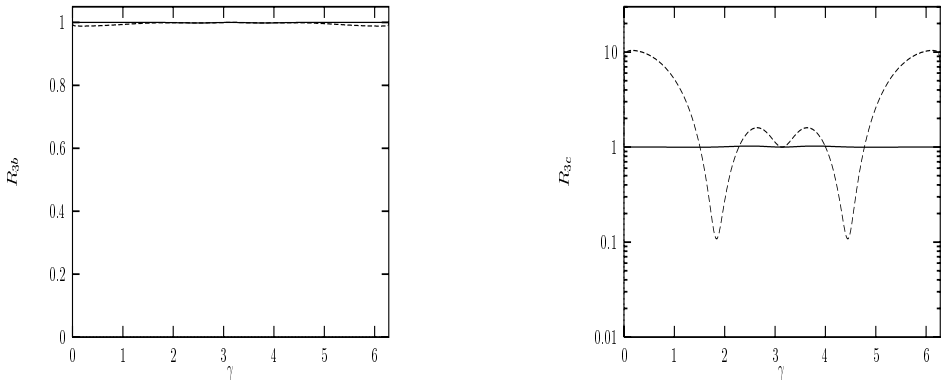

Figure 8: R_{3b} (left panel) and R_{3c} (right panel) defined in (34) as a function of γ for $\tan\beta = 4$ (solid curve) and $\tan\beta = 30$ (dashed curve).

up due to the mixing terms in the scalar mass-squared matrix which

1. are proportional to the relative phase between the two doublets,
2. increase with increasing $\tan\beta$.

- The lightest Higgs scalar remains essentially CP–even irrespective of the supersymmetric CP phases. Therefore, the MSSM has a light CP=+1 scalar as in the CP–respecting case which can, however, be distinguished from that of the CP–invariant theory, for example, by its reduced decay rate to $\bar{b}b$ pairs.

- As in the CP–invariant case, there are two heavy scalars which have

  1. definite CP quantum numbers for small $\tan\beta$ values,
  2. no definite CP characteristics for large $\tan\beta$.

- The strong mixing between the heavy scalars affect significantly their decay rates to fermion pairs, and such mixings can be important in

other collision processes testable at future colliders. Especially the decay rate of the would-be CP–odd scalar gets enhanced for $0 < \gamma \leq \pi/2$.

- The supersymmetric CP–violating phases not only cause the creation of CP–violating mixings but also modify the couplings and masses compared to ones in the CP–invariant case.

In the light of these results one concludes that the supersymmetric phases can be useful tools for obtaining manifestations of supersymmetry through their effects on collision and decay processes testable in near future colliders.

5 Acknowledgements

It is a pleasure for author to express his gratitude to A. Masiero for highly useful discussions and his careful reading of the manuscript. He would like to thank to T. M. Aliev, too, for helpful discussions.

References

[1] M. Dugan, B. Grinstein and L. J. Hall, *Nucl. Phys.* **B255** (1985) 413.

[2] S. Dimopoulos and S. Thomas, *Nucl. Phys.* **B465** (1996) 23.

[3] J. Ellis, S. Ferrara and D. V. Nanopoulos *Phys. Lett.* **B114** (1982) 231; W. Buchmüller and D. Wyler, *Phys. Lett.* **B121** (1983) 321; J. Polchinski and M. Wise, *Phys. Lett.* **B125** (1983) 393; F. del Aguila, M. Gavela, J. Grifols and A. Mendez, *Phys. Lett.* **B126** (1983) 71; D. V. Nanopoulos and M. Srednicki, *Phys. Lett.* **B128** (1983) 61; Y. Kizukuri and N. Oshimo, *Phys. Rev.* **D46** (1992) 3025; T. Falk and K. A. Olive, *Phys. Lett.* **B375** (1996) 196; T. Falk, K. A. Olive and M. Srednicki, *Phys. Lett.* **B354** (1995) 99.

[4] S. A. Abel and J. M. Frere *Phys. Rev.* **D55** (1997) 1623.

[5] T. Ibrahim and P. Nath, *Phys. Rev.* **D57** (1998) 478; *Phys. Rev.* **D58** (1998) 111301; M. Brhlik, G. J. Good and G. L. Kane, hep-ph/9810457.

[6] S. Dimopoulos and G. F. Giudice, *Phys. Lett.* **B357** (1995) 573; A. Cohen, D. B. Kaplan and A. E. Nelson, *Phys. Lett.* **B388** (1996) 599; A. Pomarol and D. Tommasini, *Nucl. Phys.* **B488** (1996) 3.

[7] D. A. Demir, A. Masiero and O. Vives, hep-ph/9812337.

[8] M. Carena and C. E. M. Wagner, hep-ph/9704347; J. M. Cline, M. Joyce and K. Kainulainen, *Phys. Lett.* **B417** (1998) 79; M. Carena, M. Quiros and C. E. M. Wagner, *Nucl. Phys.* **B524** (1998) 3.

[9] H. E. Haber and R. Hempfling, *Phys. Rev. Lett.* **66** (1991) 1815; Y. Okada, M. Yamaguchi and T. Yanagida, *Prog. Theor. Phys.* **85** (1991) 1; J. Ellis, G. Ridolfi and F. Zwirner, *Phys. Lett.* **B257** (1991) 83; *Phys. Lett.* **B262** (1991) 477; R. Barbieri and M. Frigeni, *Phys. Lett.* **B258** (1991) 395.

[10] P. Chankowski, S. Pokorski and J. Rosiek, *Nucl. Phys.* **B423** (1994) 437; A. Dabelstein, *Nucl. Phys.* **B456** (1995) 25; *Z. Phys.* **C67** (1995) 495; J. Bagger, K. Matchev, D. Pierce and R. Zhang, *Nucl. Phys.* **B491** (1997) 3.

[11] J. A. Casas, J. R. Espinosa, M. Quiros and A. Riotto, *Nucl. Phys.* **B436** (1995) 3; M. Carena, J. R. Espinosa, M. Quiros and C. Wagner, *Phys. Lett.* **B355** (1995) 209; M. Carena, M. Quiros and C. Wagner, *Nucl. Phys.* **B461** (1996) 407; H. E. Haber, R. Hempfling and A. Hoang, *Z. Phys.* **C75** (1997) 539.

[12] R. Hempfling and A. Hoang, *Phys. Lett.* **B331** (1994) 99; R.-J. Zhang, hep-ph/9808299.

[13] S. Heinemeyer, W. Hollik and G. Weiglein, hep-ph/9812472.

[14] A. Pilaftsis, *Phys. Rev.* **D58** (1998) 096010; *Phys. Lett.* **B435** (1998) 88.

[15] J. F. Gunion, H. E. Haber, G. Kane, S. Dawson, **The Higgs Hunter's Guide**, Addison-Wesley, NY (1990).

[16] M. Sher, *Phys. Rep.* **179** (1989) 273.

[17] H. E. Haber, hep-ph/9505240.

[18] J. R. Espinosa, Surveys High Energ. Phys. **10** (1997) 279.

[19] K. Funakubo, hep-ph/9809517; M. Laine, K. Rummukainen, hep-ph/9811369.